JETIR.ORG ISSN: 2349-5162 | ESTD Year : 2014 | Monthly Issue
JOURNAL OF EMERGING TECHNOLOGIES AND INNOVATIVE RESEARCH (JETIR)
An International Scholarly Open Access, Peer-reviewed, Refereed Journal

Investigation of Structural, Optical and Electrochemical Behaviors of ZnO@Ac Nanorods by Short Term Microwave – Autoclave Technique

Gunasekaran Munusamy[1], Seenuvasakumaran Perumal[2] and Rajesh V[3]*

[1, 2& 3]Department of Physics,

[1] Muthurangam Government Arts College (A), Affiliated to Thiruvalluvar University, Vellore- 632 002, Tamil Nadu, India.

[2] Government Arts and Science College, Affiliated to Thiruvalluvar University, Thirupathur– 635901, Tamil Nadu, India.

[3] Thiru Kolanjiappar Government Arts College, Affiliated to Thiruvalluvar University, Vriddhachalam – 606 001, Tamil Nadu, India.

Abstract:

Supercapacitors, an advanced technology component of electrochemical performance of energy storage technology, have attracted a lot of research and commercial interest for over a decade due to their advantages of high power density and sustained cycle stability. High-performance supercapacitors with an electrode consisting of porous carbon and metal oxide Nanorods have recently been developed and used as electrode materials in energy storage devices like removal batteries. The average crystallite size of the powder samples is 34.27 nm, according to an XRD analysis. To investigate the inherent strain and particle size using XRD peak broadening examinations, SSP, W-H plot and H-W plot techniques were applied. UV-Vis spectroscopy revealed more than 80% optical transparency with a reduced UV cutoff of 235 nm. The optical band gap was determined to be 5.12 eV. The refractive index and other optical properties were analyzed using transmission spectrum data. With some spectrum manipulation, intense PL was also seen, most likely with a range of emission photon energies from 1.83 eV. The zinc oxide powder appears have rod like structure and form of flowers in SEM photos. The electrochemical properties were investigated using cyclic voltametric technique. The specific capacitance of the ZnO@AC electrode was measured to be 660 F/g in the presence of 1M Li_2SO_4 electrolyte at a scan rate of 1 mV/s. The remarkable electrochemical performances of ZnO@AC composites contributed to the identification of these materials as high-performance materials for supercapacitor electrodes.

Keywords: XRD, SSP, W-H plot, H-W plot, ZnO@AC, etc.,

1. Introduction

Future fossil fuel depletion, as well as increasing requirements for tiny electronic devices and electric hybrid automobiles requiring enormous amounts of power in short-time pulses, have all contributed to a rise in interest in electrochemical capacitors in recent years. Supercapacitors are often referred to as electrochemical capacitors, which are excellent energy storage devices for high-power, demanding applications. They have received plenty of attention and are seen as the best candidates for the next generation of energy storage devices. Compared to batteries, it has more time between cycles, fast charging and discharging, a higher power density, high efficiency, safety, a broad working temperature range, and is friendly to the environment [1, 2]. As a result, the supercapacitor bridges the gap between batteries and typical capacitors. The majority of this research focused on C-based materials considered reliable supercapacitors, especially carbon nanotubes and activated carbon (AC), which may be attributed to superior conductivity, active surface area, high stability, porosity, and electrochemical stability [3-6].However, capacitance values are constrained by the microstructures of the materials [7, 8].

Transition metal oxides are currently attracting the interest of researchers as electrode material additions in electrochemical capacitive deionization due to their low toxicity, economic efficiency, high stability, and capacity to store more electronic charge. Several investigations have revealed suitable electrode materials based on TMOs due to their demanding applications and robust electrochemical features [9]. Because of their distinct responsibilities in comparison to other semiconductors, the II-VI group semiconductors have attracted the interest of researchers. When compared to other metal oxide materials, ZnO is an excellent choice for use in supercapacitor devices because of its significant electrochemical activity, gas sensing, photovoltaic's, low raw material cost and environmental friendliness [10-14].

2. Methods and Materials

In this investigation, a ZnO@activated carbon (AC) composite was chemically synthesized in a short term microwave – Autoclave technique. Zinc nitrate tetrahydrate, Activated carbon, PEG, acetic acid, and double-distilled water (2D water) are used in the fabrication of ZnO@AC. Zinc nitrate tetrahydrate and activated carbon were used as precursors; acetic acid and Poly Ethylene

Glycol (PEG) acted as a reducing agent and capping agent. All laboratory equipments were washed with 2D water and acetone. In 50 ml of 2D water, zinc nitrate tetrahydrate was dissolved, followed by acetic acid and activated carbon. After 2 hours, PEG was added into the beaker drop by drop. The obtained sample was transferred into an autoclave, and it is kept in a microwave for six hours. Then the synthesized sample was naturally cooled in ambient temperature. The synthesized sample was then washed multiple times with methanol and distilled water before being filtered and dried for two hours on a hot plate. The dried sample was transferred into mortar and then grained to make a fine nanoparticle using mortar. Finally, the ZnO@AC Nanorods were kept in a furnace at 800°C using a crucible to get a pure nanoparticle without any impurities. Then the prepared sample was subjected to different characterization techniques, like structural analysis using XRD, optical analysis using UV, FTIR, and PL, and surface morphology using SEM.

3. Results and discussion

3.1. X-Ray diffraction Analysis

XRD analysis was carried out to study of the crystalline nature of the fabricated ZnO/AC. The presence of peaks in XRD shown in figure 1 confirmed the crystalline nature of ZnO@AC Nanoparticles and it exhibit Hexagonal phase with the lattice parameters a=b=3.2499 Å & c=5.2061 Å and α=β=90º γ=120º respectively. The average particle size is found to be 34.27 nm using

Debye Scherrer's formula $$D = \frac{0.9\,\lambda}{\beta Cos\theta} \quad (1)$$

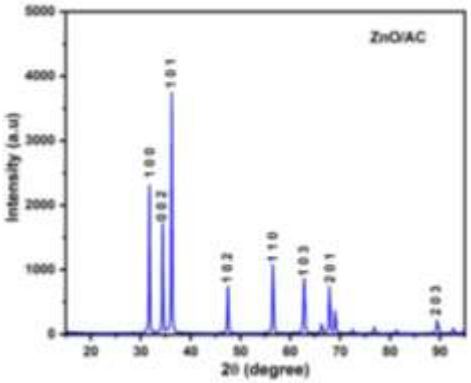

Figure 1 XRD graph of ZnO@AC Nanorods

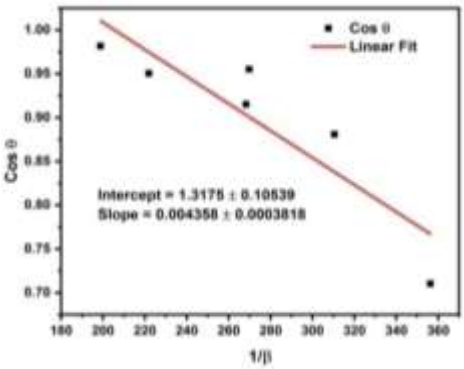

Figure 2 Straight line Scherrer Plot

Using the Debye Scherrer's equation$\cos\theta = \frac{k\lambda}{D}\left(\frac{1}{\beta}\right)$ (2)

where λ is wavelength of X-ray, β is diffraction line broadening calculated at Full-width half-maximum at its highest intensity (in radians), θ is the Bragg's diffraction angle (in degrees) D is the particle size (in nm) [15].

The modified Scherrer formula is expressed as$\frac{K\lambda}{D.\cos\theta} = \frac{K\lambda}{D}.\frac{1}{\cos\theta}$ (3)

Using the logarithm on both sides$\beta = \ln\left(\frac{K\lambda}{D.\cos\theta}\right) = ln\left(\frac{K\lambda}{D}\right) + ln\left(\frac{1}{\cos\theta}\right)$ (4)

By graphing ln β and ln (1/cos θ) (Fig. 3), straight line with an intercept equal to ln (Kλ/D) is used to calculate particle size 32.58 nm is obtained.

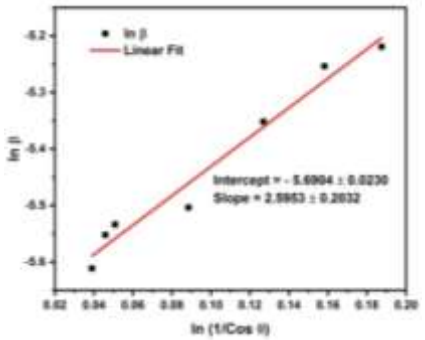

Figure 3 Modified Scherrer Plot

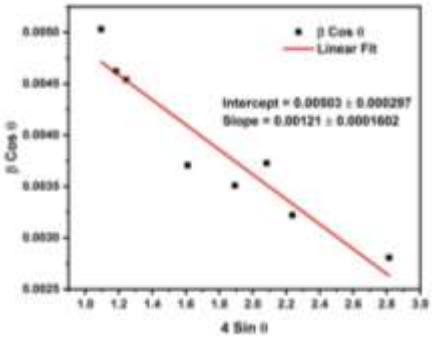

Figure 4 W-H Plot of ZnO@AC Nanorods

The W-H plot is a reduced integral breadth approach that does not depend on 1/cos θ as the Scherrer method does but rather changes with tan θ. The strain impact on the line broadening of the diffraction peak is given by

$$\varepsilon = \frac{\beta}{4\tan\theta} \quad (5)$$

Where ε is maximum lattice strain and the particle size is found to be 29.29 nm [16].

The dislocation density can be defined as the number of dislocation points per unit volume of the crystal. In the investigation of materials, a dislocation is a defect or imperfection in the crystal structure. The existence of dislocations has a major effect on several material properties. As a result, a high dislocation density suggests a higher hardness [16]. Dislocation density of the sample can be expressed by the equation are

$$\delta = \frac{15\,\beta\cos\theta}{4aD} \tag{6}$$

Where δ is the dislocation density, a is the lattice constant.

The density of dislocations may also be calculated using $\delta = \frac{1}{D^2}$ (7)

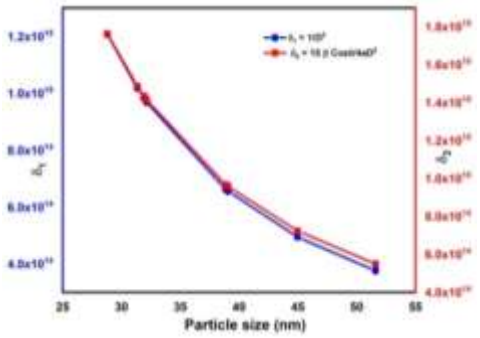

Figure 5 Dislocation Density graph

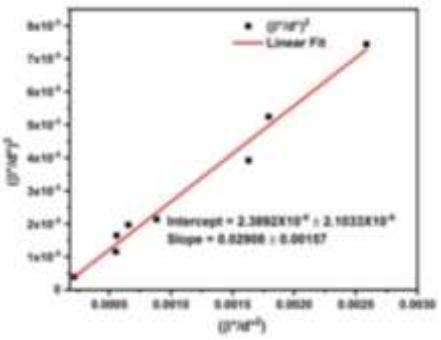

Figure 6 H-W plot of ZnO@AC Nanorods

In Halder Wagner's method, Gauss and Lorentzian functions are used to determine strain and average crystallite size profiles.

$$\left(\frac{\beta^*}{d^*}\right)^2 = \frac{1}{D}.\frac{\beta}{d^2} + \left(\frac{\varepsilon}{2}\right)^2 \tag{8}$$

Where d is the interplanar distance between planes [17]. Figure 6 shows the HW plot. From the graph y-intercept of the plot from linear fitted data gives the average value of the strain and the slope gives the crystallite size. The advantage of this graph is that data for reflections at low and mid-angles are given greater significance than data for reflections at higher angles, where accuracy is frequently lower.

The size-strain plot approach is employed to account for the isotropic character of the crystal structure. A Gaussian function is meant to represent the strain profile, while a Lorentzian function is expected to explain the crystallite size profile.

$$(d_{hkl}\beta_{hkl}Cos\theta)^2 = \frac{K}{D}(d_{hkl}\beta_{hkl}Cos\theta)^2 + \left(\frac{\varepsilon}{2}\right)^2 \tag{9}$$

Figure 7 the graph is drawn between $(d^2 * \beta^2 Cos\,\theta)$ and $(d * \beta Cos\theta)^2$[18]. From the graph the slope implies the size of the crystallite is 31.27 nm, whereas the y-intercept indicates the strain value is 0.00164.

The Lorentz-polarization factor is the experimental variable that most strongly influences how the diffraction angle affects X-ray intensity. In the intensity calculations, the Lorentz factor is coupled with the polarization factor and the shift of the Lorentz factor with the Bragg angle (θ) can be observed [19,20]. In respect of reflections in either forward or backward directions, the Lorentz factor reduces the intensity of reflections at intermediate angles.

$$\text{Lorentz Factor} = \frac{\cos\theta}{sin^2\,2\theta} = \frac{1}{4sin^2cos\,\theta} \tag{10}$$

$$\text{Polarization factor} = \left(\frac{1+cos^2(2\theta)}{sin^2\theta\,cos\theta}\right) \tag{11}$$

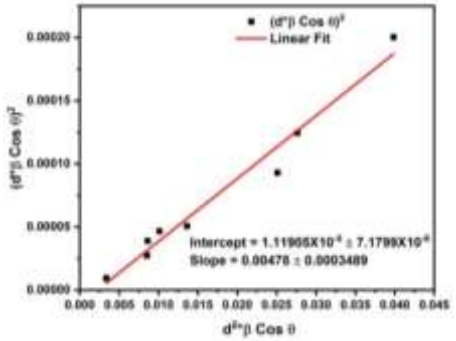

Figure 7 SSP plot of ZnO@AC Nanorods

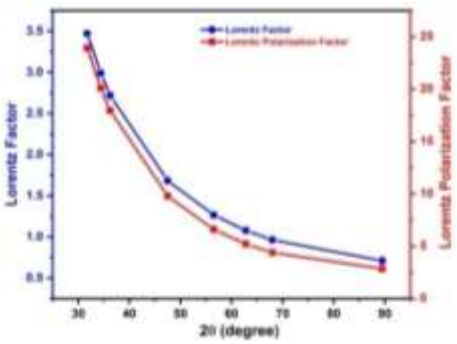

Figure 8 Lorentz factor and Polarization factor

3.2 Optical Properties

Optical characterization is a significant factor to consider when evaluating the quality of crystalline materials. Optical transmission in the UV region decreases at lower wavelengths due to energy absorption caused by the electrical shift from the valance band to the unfilled conduction band.

Figure 9 display the plot of absorption and % transmission versus wavelength (nm). ZnO@AC Nanorods have low cutoff wavelength and fairly high transparency window it exhibit good optical quality.

The absorption coefficient of ZnO@AC Nanorods can be determined by $\alpha = \frac{2.303\ A}{l}$ where A is absorption and l is the thickness. Figure 10 shows the graph between Absorption coefficient and wavelength.

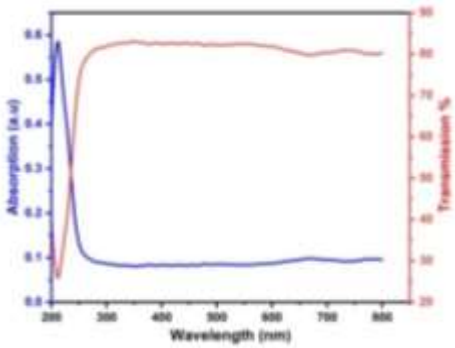

Figure 9 Absorption, Transmission vs wavelength

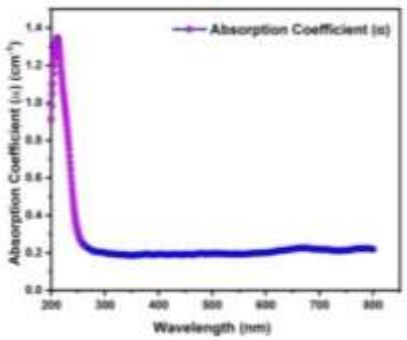

Figure 10 Absorption coefficient Vs wavelength

To determine the band gap using optical absorbance data, Tauc plot is a reliable method. A semiconductor's optical energy band gap can be calculated by measuring the material's absorption of incident photons. The optical absorption intensity can be evaluated experimentally using the absorption co-efficient; the formula for the photon energy dependence of the absorption co-efficient for direct and indirect transitions is given below.

$$\alpha = \frac{A(h\nu - E_g)^n}{h\nu} \qquad (12)$$

Here the optical band gap is Eg, the Planck's constant is h, and the frequency of the incoming photons A is constant. The value of Eg obtained from the absorption analysis was 5.12 eV, as shown in Figure 11. The dielectric behavior of the ZnO@AC Nanorods is suggested by the comparatively large band gap value and the wide transparency window [21, 22].

Refractive index from the transmittance value of ZnO@AC Nanorods is determined from the equation

$$n = \frac{1}{T} + \sqrt{\left(\frac{1}{T} - 1\right)} \qquad (13)$$

Figure 12 shows the change in refractive index with wavelength for ZnO@AC Nanorods. As the wavelength rises, the refractive index falls. The ZnO@AC Nanorods is useful for optoelectronic applications due to its greater band gap, strong transmission in the general area, and reduced refractive index [23].

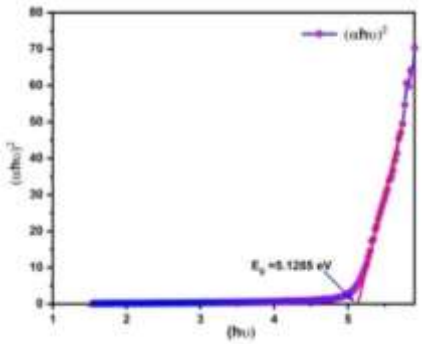

Figure 11 Energy band gap of ZnO@AC Nanorods

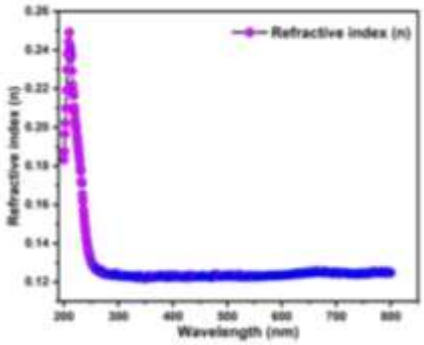

Figure 12 Refractive index of ZnO@AC Nanorods

3.3 Photoluminescence Analysis:

Light emission from compound semiconductors has been an important phenomenon due to its practical applications. The vast majority of optoelectronic devices, among the light-emitting diodes, are constructed with semiconductors that have linear band gap transitions and high efficiency [24]. Figure 5, the photoluminescence spectrograph shows the emission peaks for ZnO@AC Nanorods ranging from 300 to 900 nm.

As a result of photon transitions, the emission wavelength is 656.85 nm, which produces visible yellow light 417.46 nm and 482.29 nm, respectively. The energy band of PL emission wavelength is 1.83 eV.

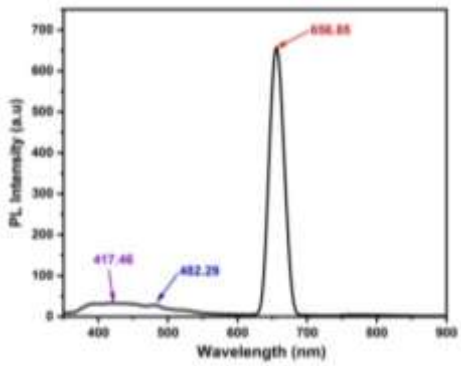

Figure 13 PL Emission wavelengths of ZnO@AC Nanorods

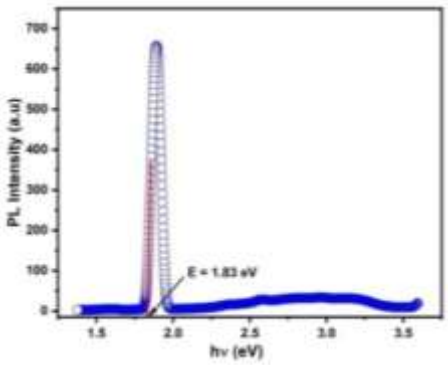

Figure 14 PL Energy band gap of ZnO@AC Nanorods

3.4 Electrochemical Analysis

The electrochemical characteristics of the ZnO@AC composites were evaluated using a three-electrode cell arrangement with a 1 M Li_2SO_4 electrolyte through the potential range of -0.2 to 0.2 V. Scan speeds at the rate of 1mV/s to 100 mV/s, the cyclic voltammograms (CV) of ZnO@AC electrode samples are shown in Figures 15. The ZnO@AC Nanorods show rectangular shape even at these high scan speeds. Figure 16 shows the specific capacitances of ZnO@AC were determined using the formula

$$C_s = \frac{I\Delta t}{m\Delta V} \qquad (14)$$

Where I is the applied current, m is the mass of the material electrode, ΔV - the potential window of charging and discharging is processes in volts, and Δt - the discharge period to be 660 F/g using galvanostatic charge-discharge at a current density of 1 A/g, respectively. The ZnO@AC nanoparticles are excellent for supercapacitors due to their long-term cyclic stability, which includes good charge transfer, rapid ion diffusion, low contact resistance with potential change, low cost, and high electrochemical performance.

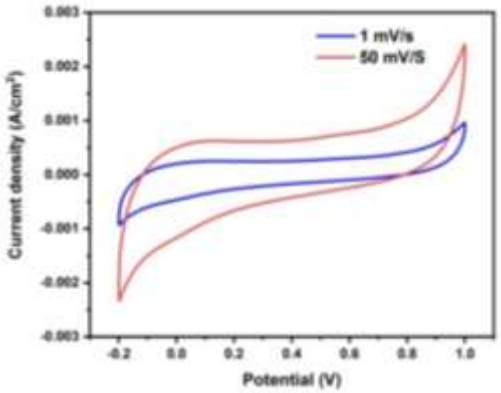

Figure 15Current density graph of ZnO@AC Nanorods

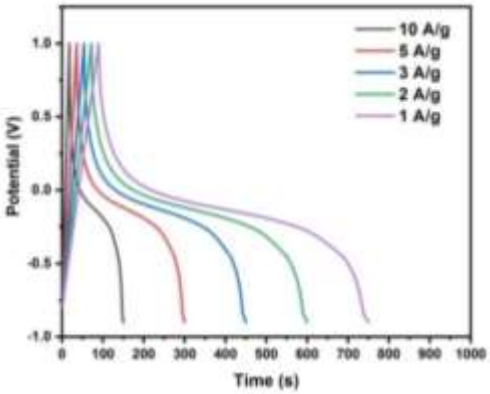

Figure 16GCD graph of ZnO@AC Nanorods

3.5 Surface Morphology

Figure 17 shows the morphology analysis of synthesized ZnO@AC Nanorods using scanning electron microscope at different scale range 1µm, and 200 nm. It shows nano rod like structure, some parts of images shows flower and plate like structure. This unique morphology surface has high supercapacitor application.

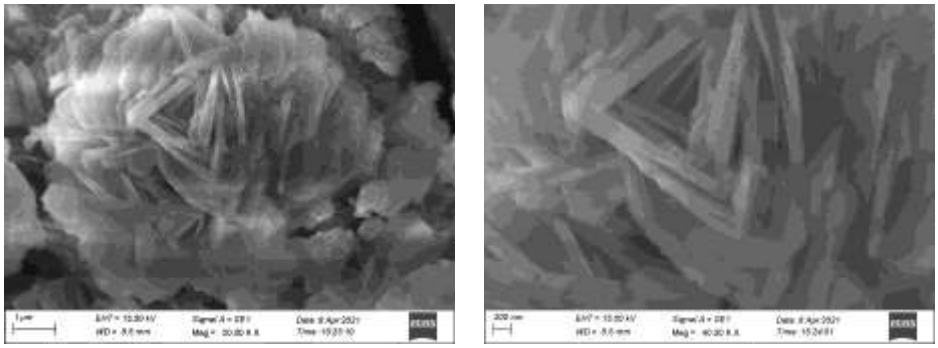

Figure 17 SEM images of ZnO@AC Nanorods

4. Conclusions

In the present investigation, short term microwave – Autoclave technique was used to efficiently synthesize hexagonal ZnO@AC Nanorods with a narrow range of size and rod shape, which were then characterized using various methods such as XRD, UV-Vis, PL, Electrochemical analysis, and SEM. The investigations have also verified the composite formation. Using various approaches, the average size of the particles of ZnO@AC Nanorods is determined to be 29.29 nm to 34.27 nm. The UV spectral study demonstrated a decreased UV cutoff at 245nm with a broad transparency window. The calculation of the optical energy band gap (Eg) and refractive index from the UV spectrum suggests that the material is suitable for optoelectronic applications. Intense PL was also detected with some spectrum modification, most likely with a range of its emission red and yellow colors and photon energies ranging from 1.83 eV. The ZnO@AC electrodes have a specific capacitance of around 660 F/g at 1 A/g. All of the results suggested that the relationship between surface area and porosity of activated carbon and ZnO composites may be optimized for commercial usage as electrode materials for supercapacitors.

Reference:

1. P. Simon, Y. Gogotsi, Materials for electrochemical capacitors.Nat. Mater. **7**, 845–854 (2008)
2. C. Liu, F. Li, L. Ma, H. Cheng, Advanced materials for energystorage. Adv. Mater. **22**, E28–E62 (2010).
3. K.S. Lee, C.W. Park, J.-D. Kim, Synthesis of ZnO/activated carbon with high surface area for supercapacitor electrodes, Colloids and Surfaces A: Physicochemical and Engineering Aspects, 555 (2018) 482-490.
4. T. Yumak, D. Bragg, E.M. Sabolsky, Effect of synthesis methods on the surface and electrochemical characteristics of metal oxide/activated carbon composites for supercapacitor applications, Applied Surface Science, 469 (2019) 983-993.
5. Q. Zhou, T. Fan, Y. Li, D. Chen, S. Liu, X. Li, Hollow–structure NiCo hydroxide/carbon nanotube composite for High–Performance supercapacitors, Journal of Power Sources, 426 (2019) 111-115.
6. Q. Wang, Y. Ma, X. Liang, D. Zhang, M. Miao, Flexible supercapacitors based on carbon nanotube-MnO2 nanocomposite film electrode, Chemical Engineering Journal, 371 (2019) 145-153.
7. L.L. Zhang, X.S. Zhao, Carbon-based materials as supercapacitor electrodes, Chem. Soc. Rev. 38(9) (2009) 2520-2531.
8. D.N. Futaba, K. Hata, T. Yamada, T. Hiraoka, Y. Hayamizu, Y. Kakudate, Shapeengineerable and highly densely packed single-walled carbon nanotubes and their application as super-capacitor electrodes, Nat. Mater. 5(12) (2006) 987-994.
9. R. Liu, D. Zhao, L. Duan, X. Zhao, Optical and photo catalytic properties of $Zn_{1-x}Cd_xO$ nanoparticles with tuned oxygen vacancy, *Journal of Alloys and Compounds* (2020).
10. D. Kalpana, K.S. Omkumar, S.S. Kumar, N.G. Renganathan, A novel high power symmetric ZnO/carbon aerogel composite electrode for electrochemical supercapacitor, Electrochim. Acta 52 (2006) 1309.
11. M. Selvakumar, D.K. Bhat, A.M. Aggarwal, S.P. Iyer, G. Sravani, Nano ZnOactivated carbon composite electrodes for supercapacitors, Phys. B 405 (2010) 2286.
12. L.S. Aravindaa, K.K. Nagarajab, H.S. Nagarajab, K.U. Bhat, B.R. Bhat, ZnO/carbon nanotube nanocomposite for high energy density supercapacitors, Electrochim. Acta 95 (2013) 119.
13. Y. Zhang, X. Sun, L. Pan, H. Li, Z. Sun, C. Sun, B.K. Tay, Carbon nanotube-ZnO nanocomposite electrodes for supercapacitors, Solid State Ionics 180 (2009) 1525.
14. S. Rajaboopathi, S. Thambidurai, Heterostructure of CdO-ZnO nanoparticles intercalated on PANI matrix for better thermal and electrochemical performance, Materials Science in Semiconductor Processing 59 (2017) 56–67.
15. Gunasekaran M, Jayapriya J and Seenuvasakumarn P, Structural, Optical and Magnetic Studies of CdTiCoFe2O4 Nanoparticles bySol-Gel Method, *Elixir Materials Science, 86 (2015) 35014-350.*
16. R.Hepzi Pramila Devamani and M.Alagar Synthesis and Characterization of Copper II Hydroxide Nano Particles, *Nano Biomed. Eng.* 2013, 5(3), 116-120.
17. L Motevalizadeh, Z Heidary and M Ebrahimizadeh Abrishami, Facile template-free hydrothermal synthesis and microstrain measurement of ZnO nanorods, *Bull. Mater. Sci.*, Vol. 37, No. 3, May 2014, pp. 397–405.
18. A. Khorsand Zak, W.H. Abd. Majid, M.E. Abrishami, Ramin Yousefi, X-ray analysis of ZnO nanoparticles by WilliamsoneHall and sizeestrain plot methods, *Solid State Sciences* 13 (2011) 251-256
19. Mark Ladd Rex Palmer, Structure Determination by X-ray Crystallography Analysis by X-rays and Neutrons, *Fifth Edition, Springe.*
20. Sumit Sarkar & Ratan Das, Determination of structural elements of synthesized silver nano-hexagon from X-ray diffraction analysis, *Indian Journal of Pure & Applied Physics* Vol. 56, October 2018, pp. 765-772.
21. J. Tauc, A. Menth, and D. L. Wood, "Optical and Magnetic Investigations of the Localized States in Semiconducting Glasses," *Physical Review Letters*, vol. 25, no. 11, pp. 749–752, 1970.
22. N. A. Bakr, A. M. Funde, V. S. Waman et al., "Determination of the optical parameters of a-Si:H thin films deposited by hot wire-chemical vapour deposition technique using transmission spectrum only," *Pramana—Journal of Physics*, vol. 76, no. 3, pp. 519–531, 2011.
23. J. H. Joshi, S. Kalainathan, D. K. Kanchan, M. J. Joshi, K. D. Parikh, and J. Arabian, "Effect of l-threonine on growth and properties of ammonium dihydrogen phosphate crystal," *Arabian Journal of Chemistry*, 2017.
24. Munusamy Gunasekaran, Seenuvasakumaran Perumal "Lead oxide and vanadium doped lead oxide thin films for optoelectronic device applications", *Materials Today: Proceedings 47(1-2)*, August 2021.